COBEM 2023 27TH INTERNATIONAL CONGRESS OF MECHANICAL ENGENEERING

ABCM Brazilian Society of Mechanical Sciences and Engineering
27th ABCM International Congress of Mechanical Engineering
December 04-08, 2023, Florianópolis-SC, Brazil

COB-2023-0223
Investigation of shock-boundary layer interactions in a supersonic turbine cascade under different inlet Mach numbers

Hugo F. S. Lui
William R. Wolf
Universidade Estadual de Campinas
Rua Mendeleyev, 200 - Cidade Universitária, Campinas - SP, 13083-860, Brazil
hugo.slui@gmail.com
wolf@fem.unicamp.br

Tulio R. Ricciardi
University of Illinois Urbana-Champaign
1205 W Clark St, Urbana, IL 61801, United States
tulioricci@gmail.com

Abstract. *The effects of inlet Mach number on shock-boundary layer interactions (SBLIs) in a supersonic turbine cascade at Reynolds number 395,000, based on the axial chord, are studied using large eddy simulations and post-processing techniques. Three values of Mach number are considered 1.85, 2.00 and 2.15. Particular emphasis is placed on understanding the effects of inlet Mach number on the unsteadiness of the bubble/shock system. The present configuration depicts some differences on the shock structure when compared to canonical cases (impinging oblique shock on a flat plate and compression ramp) due to the curved walls of the turbine. On the suction side, an oblique shock interacts with the boundary layer, while a Mach reflection is formed on the pressure side. Flow visualizations and an analysis of the mean flow show that a higher inlet Mach number leads to a stronger leading edge bow shock that in turn generates a more inclined oblique shock, resulting in a downstream displacement of the SBLI region on both sides of the airfoil. A side consequence of the topological changes is an increase of the suction side separation bubble length as the inlet Mach number is increased. This effect is less pronounced on the pressure side, where the recirculation regions have similar lengths. Finally, the separation bubble dynamics is investigated using spectral analysis for all cases. The results indicate that, as the inlet Mach number increases, the regions with high-spectral energy at low-frequencies move downstream in the axial direction, and the SBLI systems excite even lower frequencies.*

Keywords: *Shock-Wave Boundary Layer Interactions, Supersonic Flow, Turbine, Large Eddy Simulation*

1. INTRODUCTION

Supersonic turbines can be employed in high-speed propulsion and power generation systems (Sousa *et al.*, 2017; Paniagua *et al.*, 2014), and also in hydrocarbon cracking plants (Rubini *et al.*, 2021). The analysis of internal supersonic flows is dificult due to the shock reflections and shock-boundary layer interactions (SBLIs) that occurs when oblique shock waves produced at the airfoil leading edges interacts with the turbulent boundary layers of the neighboring airfoils (Lui *et al.*, 2022). The incident shocks impose intense adverse pressure gradients on the boundary layers that cause flow separation, resulting in the formation of compression waves and reattachment shocks. The combination of these flow features can increase total pressure losses in the internal passage and induce higher heat transfer rates to the blade surface, thus resulting in reduction of the overall system efficiency (Gaitonde, 2015). Moreover, the coupling of intense thermal and pressure loads can compromise the blade structural integrity (Klinner *et al.*, 2019; Sandberg and Michelassi, 2022).

SBLIs are a source of intense flow unsteadiness and excite a broad range of frequencies. Several researchers have studied the low-frequency events that occur in supersonic compression ramps and impinging shock flows using numerical (Pirozzoli and Grasso, 2006; Touber and Sandham, 2009; Priebe and Martín, 2012; Adler and Gaitonde, 2018) and experimental (Dussauge *et al.*, 2006; Dupont *et al.*, 2006; Ganapathisubramani *et al.*, 2009) techniques. Based on previous studies, the flow unsteadiness can be classified into different frequency bands, depending on the Strouhal number: low frequency oscillations from the reflected shock motion and large-scale bubble breathing ($0.02 < St_{LSB} < 0.05$), low to mid-frequency motions of the separation bubble and flapping of the shear layer ($St_{LSB} \approx 0.1$), and the Kelvin-Helmholtz (KH) instabilities ($0.3 < St_{LSB} < 0.5$). Here, the Strouhal number $St_{LSB} = fL_{SB}/U_\infty$ is defined based on the length of the separation bubble L_{SB} and the inlet velocity U_∞. Although the low-frequency dynamics of the SBLIs has been well described, its source is still a subject of debate because the driving mechanisms have not been fully elucidated (Clemens and Narayanaswamy, 2014). Some studies have shown that the upstream boundary layer fluctuations are responsible for

the low-frequency unsteadiness (Beresh *et al.*, 2002; Ganapathisubramani *et al.*, 2009; Porter and Poggie, 2019; Baidya *et al.*, 2020), while other investigations have associated them with a global instability of the separation bubble (Touber and Sandham, 2009; Nichols *et al.*, 2017; Adler and Gaitonde, 2018).

Most of the previous studies have investigated the physics of SBLIs in a single set of flow conditions, and only a limited number of studies covered parametric variations such as the inlet Mach number, wedge angle and Reynolds number. Dupont *et al.* (2006) experimentally investigated a Mach 2.3 shock impinging on a turbulent boundary layer for a wide range of shock intensities by varying the wedge angle. Their results suggest that the length of the interaction zone (normalized by the incoming boundary layer displacement thickness) increases with the shock intensity, which is defined as the ratio between the pressure jump across the incident shock and the wall-shear stress upstream of the interaction. Morgan *et al.* (2013) performed several high-fidelity simulations of a Mach 2.28 shock impinging on a turbulent boundary layer varying the Reynolds number and wedge angle. Considering the cases with constant wedge angle but changing the Reynolds number, the authors observed that the length of the separation bubble is not significantly affected by this parameter over the range considered. With regard to the effects of varying the wedge angle at a fixed Reynolds number, they reported that a stronger incident shock leads to a larger separation region, but this relationship appears to be nonlinear. The results also indicate that increasing the shock strength leads to more intense low-frequency oscillations of the SBLI system.

In the present work, we provide an assessment of shock-boundary layer interactions in a supersonic turbine cascade at Reynolds number Re = 395,000 based on the axial chord and inlet velocity. Different inlet Mach numbers are investigated, including $M_\infty = 1.85$, 2.00 and 2.15. In Sections 2 and 3, the numerical methodology and the flow configurations are described. Results are then presented in Section 4, where instantaneous and mean flow visualizations are displayed to highlight the formation of different SBLIs due to Mach number variations. The mean flow quantities are also analyzed to emphasize the implications of distinct inlet conditions on the pressure variations along the interaction zone and separation bubble size. Finally, a spectral analysis is performed to categorize the characteristic frequencies in each case, as well as to investigate the effects of the inlet Mach number on the low-frequency unsteadiness. Understanding the role of inflow variations on the SBLIs for the present configuration can provide insights for the development of efficient supersonic fluid machinery.

2. NUMERICAL METHODOLOGY

Large eddy simulations are performed using a in-house code, which solves the non-dimensional compressible Navier-Stokes equations in general curvilinear coordinates. The fluid is considered to be a calorically perfect gas, where the molecular viscosity is computed by the Sutherland's law. The spatial discretization of the governing equations is performed using a sixth-order accurate finite-difference compact scheme implemented on a staggered grid (Nagarajan *et al.*, 2003). A sixth-order compact interpolation scheme is also employed to obtain flow quantities on the different nodes of the staggered grid configuration.

An overset mesh procedure with two overlapping grids is used in the present simulations. A body-fitted O-grid block surrounds the airfoil and a H-grid block is employed to facilitate the application of the cascade pitchwise periodicity. In the O-grid, the time integration of the equations is carried out by the implicit second-order scheme of Beam and Warming (1978) to overcome the stiffness problem arising from the fine boundary layer grid. In the H-grid block, a third-order Runge-Kutta scheme is applied for time advancement of the governing equations. A fourth-order Hermite interpolation scheme (Bhaskaran and Lele, 2010) is employed to exchange information between grid blocks in the overlapping zone. An explicit subgrid scale model is not employed, however, away from the airfoil surface, a sixth-order compact filter (Lele, 1992) is used at each time step to control high wavenumber numerical instabilities arising from mesh stretching and interpolations between overlapping grids.

A proper shock capturing scheme is required to introduce a minimal numerical dissipation in the vicinity of the shock waves without damping the small scales of turbulence. In this work, the localized artificial diffusivity (LAD) (Cook, 2007) is employed to compute the artificial fluid properties, which are added to their physical transport counterparts. The specific implementation used is the method LAD-D2-0 proposed by Kawai *et al.* (2010) without adding artificial shear viscosity. To promote the transition to turbulence on the boundary layers, we apply a body forcing on the right-hand side of the Navier-Stokes equations, as described in Refs. (Sansica, 2015; Waindim and Gaitonde, 2016). Here, an unsteady actuation with a random spanwise treatment is considered and the amplitude of the disturbances is chosen to guarantee a bypass transition with minimal flow disturbance. More details about the governing equations and numerical procedure for the large eddy simulations can be found in (Lui *et al.*, 2022; Nagarajan *et al.*, 2003; Bhaskaran and Lele, 2010).

3. FLOW CONFIGURATION

This section presents details of the flow configurations investigated and describes the computational grid used in the calculations. More details about the airfoil geometry can also be found in (Liu *et al.*, 2019). Figure 1 (a) shows the geometrical parameters of the turbine cascade and the inlet flow conditions. In the present analysis, three simulations are

performed, where the Reynolds number based on the inlet velocity and axial airfoil chord c_x is fixed at $Re = 395,000$. The vane cascade is subjected to a uniform flow with three different inlet Mach numbers, including $M_\infty = 1.85$, 2.00, and 2.15. The ratio of specific heats is $\gamma = 1.31$, the Prandtl number is $Pr = 0.747$, and the ratio of the Sutherland constant over the inlet temperature is 0.07182. These conditions are chosen based on previous studies (Liu *et al.*, 2019; Lui *et al.*, 2022).

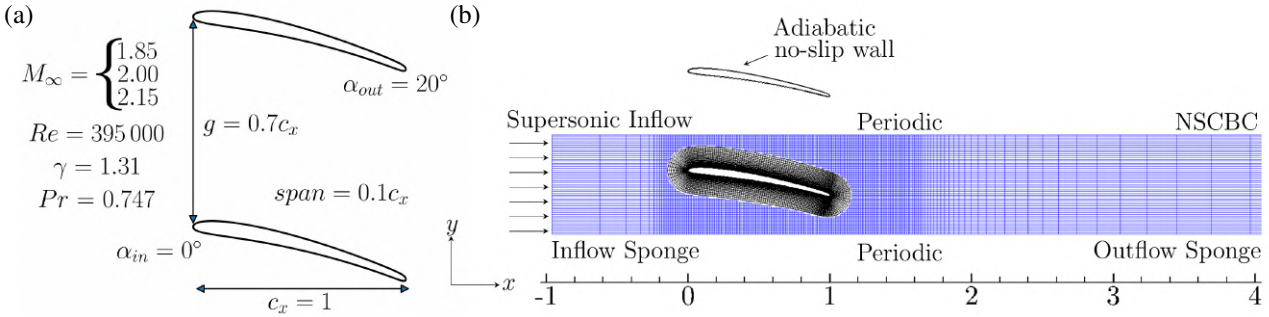

Figure 1. Schematics of (a) flow configuration and geometrical parameters, and (b) computational domain skipping every **5** grid points and boundary conditions.

Figure 1 (b) displays a schematic of the overset grid used in all calculations, along with the employed boundary conditions. The body-fitted O-grid block has $1280 \times 300 \times 144$ points in the streamwise, wall-normal and spanwise directions, respectively. The O-grid is embedded in a background Cartesian grid block of size $960 \times 280 \times 72$. Overall, the computational mesh is composed of approximately 75×10^6 points. No-slip adiabatic boundary conditions are applied along the airfoil surface. A supersonic inflow boundary condition is employed to set the inlet conditions, while the Navier-Stokes characteristic boundary conditions (NSCBC) (Poinsot and Lele, 1992) are used at the outflow. A damping sponge is also applied near the inflow and outflow boundaries to minimize reflection of numerical disturbances (Israeli and Orszag, 1981; Nagarajan *et al.*, 2003; Lui *et al.*, 2022). Periodic boundary conditions are used in the y-direction of the background grid to simulate a linear cascade of vanes. To avoid the modeling complexities near the tip and end-wall, periodic boundary conditions are also applied in the spanwise direction. The spanwise extent of the computational domain is equal to 10% of the axial chord.

4. RESULTS

In this section, we present results obtained by the large eddy simulations computed for $M_\infty = 1.85$, 2.00, and 2.15. The simulations were performed on the Stampede 2 machine at the Texas Advanced Computing Center, and on the Anvil machine at the Purdue Research Computing. In all cases, flow quantities are collected for 30 flow-through times (equivalent to $\approx$ 1.5 million CPU hours) based on the inlet velocity and blade axial chord. Here, the effects of inlet Mach number on the SBLIs in a supersonic turbine cascade are investigated using flow visualization, mean flow quantities, and spectral analysis.

4.1 Analysis of instantaneous and mean flows

Figure 2 shows iso-surfaces of Q-criterion colored by the u-velocity component together with a background view of density gradient magnitude, $|\nabla\rho|$, for (a,b) $M_\infty = 1.85$, (c,d) $M_\infty = 2.00$, and (e,f) $M_\infty = 2.15$. The left column plots display the flow through the turbine cascade, while those on the right column show detail views of the SBLIs on both sides of the airfoil. In all cases, we can observe detached oblique shock waves generated at the airfoil leading edges, and their interactions with the boundary layers of the neighboring airfoil. On the suction side, an oblique shock impinges on the turbulent boundary layer, while on the pressure side, the incident shock wave becomes normal to the wall due to a Mach reflection.

An increase in the inlet Mach number leads to different shock angles and, therefore, different impingement locations of the incident shock, causing a downstream displacement of the SBLI region on both airfoil sides. For the $M_\infty = 1.85$ case, two SBLIs are observed on the suction side. The first is due to the oblique shock formed at the blade leading edge, and the second is due to the reflected shock on the pressure side of the adjacent blade. The latter interacts with the boundary layer near the trailing edge region and also with the separation bubble formed due to the blunt trailing edge. For both $M_\infty = 2.00$ and 2.15 cases, a single SBLI occurs on the suction side. For the higher inlet Mach number, the stronger leading edge bow shock results in a more inclined oblique shock impinging on the surface, close to the airfoil trailing edge. As a consequence, a more complex interaction is observed between the shock wave, boundary layer and the trailing edge separation bubble.

To highlight the influence of the inlet Mach number on the size and shape of the mean separation bubbles, the spanwise

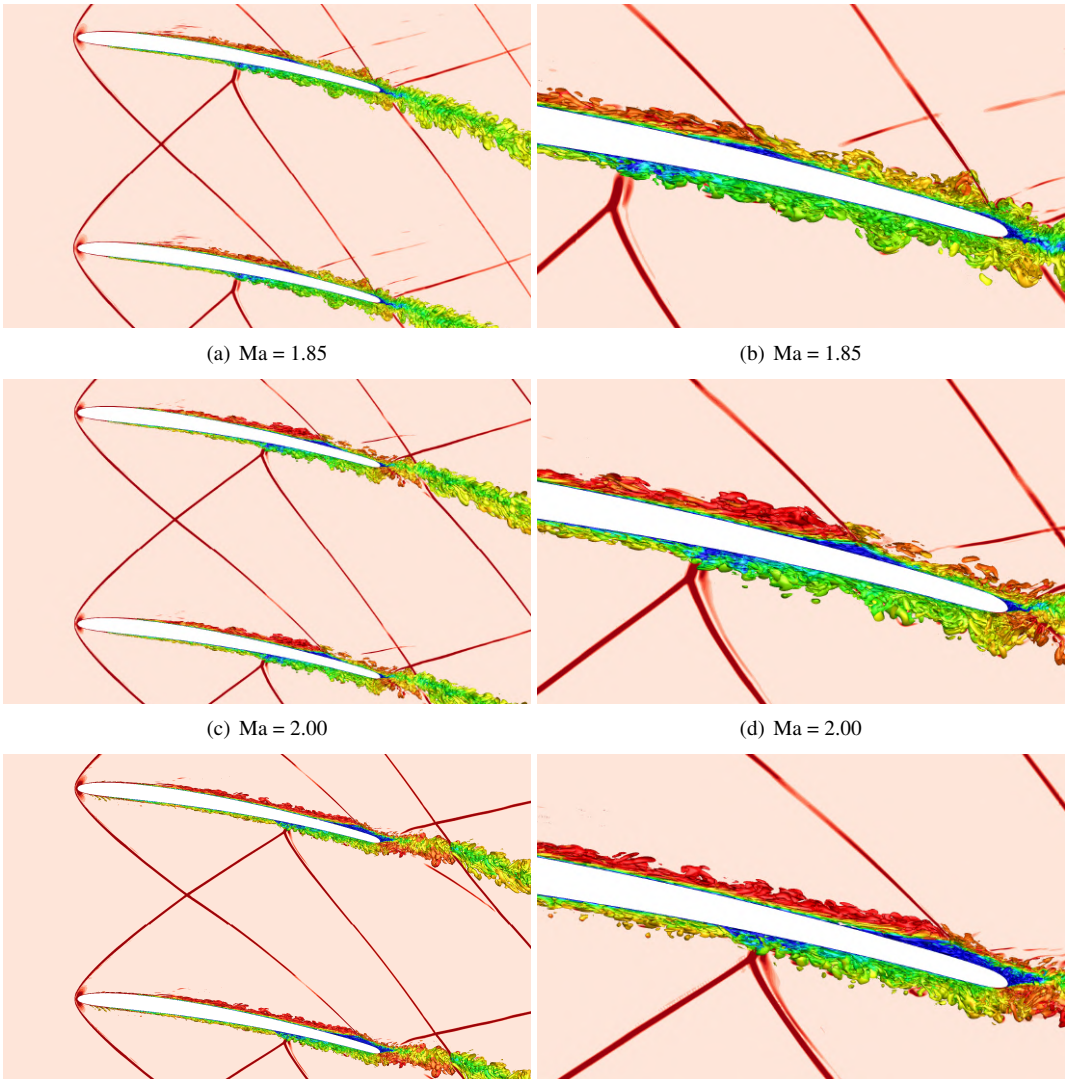

(a) Ma = 1.85 (b) Ma = 1.85

(c) Ma = 2.00 (d) Ma = 2.00

(e) Ma = 2.15 (f) Ma = 2.15

Figure 2. Iso-surfaces of $\mathbf{Q}$-criterion colored by $\mathbf{u}$-velocity component displaying the cascade (left), and a detail view of the SBLIs (right) for different inlet Mach numbers. The background plane displays the shock waves by visualizing the density gradient magnitude $|\nabla\rho|$.

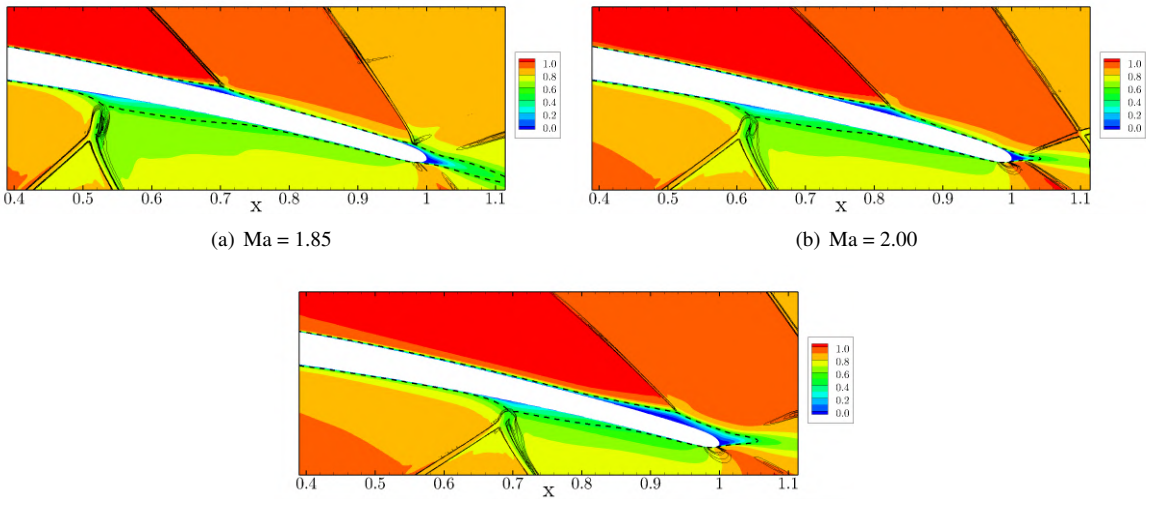

(a) Ma = 1.85 (b) Ma = 2.00

(c) Ma = 2.15

Figure 3. Spanwise and time averaged contours of streamwise velocity component u/u_∞. The black lines display the shock waves visualized by the pressure gradient magnitude, and the black dashed lines show the sonic line.

and time averaged u-velocity contours are presented in Figs. 3(a), (b) and (c). In these figures, the black dashed lines show the sonic line. The size and shape of the suction side separation bubble are significantly affected by the Mach number variation, shock angle and impingement location. On the suction side, one can also see that a higher inlet Mach number leads to an increase in the mean separation bubble length, while on the pressure side, similar separation bubbles are visualized for different Mach number. Moreover, it can be observed a displacement of the sonic line towards the wall for a lower inlet Mach number. On the other hand, the opposite behavior is true for the pressure side. It is also interesting to note that the presence of a SBLI near the trailing edge affects its separation bubble, which in turn changes the wake flow direction, and trailing-edge shock location.

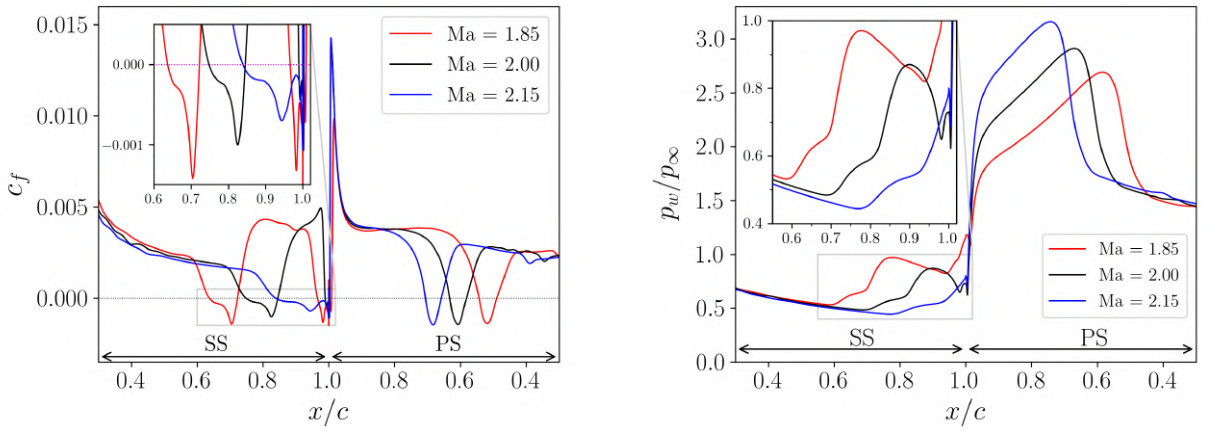

(a) Skin friction coefficient c_f

(b) Wall pressure p_w/p_∞.

Figure 4. Spanwise and time averaged (a) skin-friction coefficient and (b) wall pressure distributions for different inlet Mach numbers. Suction side (SS): upstream of $1.0\,x/c$; pressure side (PS): downstream of $1.0\,x/c$.

The chordwise distribution of the spanwise and time-averaged skin-friction coefficient, defined as

$$c_f = \frac{\tau_w}{0.5\rho_\infty U_\infty^2}\,, \tag{1}$$

is shown in Fig. 4(a) for different inlet Mach numbers. Here, τ_w represents the wall shear stress and ρ_∞ is the inlet density. The left side of the figure displays the suction side (SS) while the right side shows the c_f distribution on the pressure side (PS). The inset shows the regions with separated boundary layers on the suction side. The separation bubble location is characterized by regions where $c_f < 0$. On the suction side, one can notice that increasing the inlet Mach number causes the skin-friction coefficient of the incoming boundary layer to decrease slightly. As also noticed by the flow visualizations, as the inlet Mach number is increased, the size of the separation bubble increases and a downstream displacement of the separation region is observed. On the pressure side, the values of cf in the incoming boundary layer are similar for all cases, as well as the mean separation bubble lengths.

Figure 4(b) displays the spanwise and time averaged wall pressure distribution p_w/p_∞ along the airfoil chord. The suction and pressure sides are shown, respectively, on the left and right-hand sides. Here, the inset shows the pressure variation along the suction side bubble. For all cases, two regions of pressure rise are evident: the first near the separation location due to compression waves, and the second near the reattachment point as a result of the incident shock. Moreover, as the inlet Mach number is increased, the pressure rise becomes smoother, with a higher pressure jump observed at the lower inlet Mach number. On the other hand, on the pressure side, the Mach reflection induces a steeper rise in pressure, where increasing the inlet Mach number also increases the pressure jump.

4.2 Spectral analysis

To further characterize the effects of the inlet Mach number on the low-frequency unsteadiness, the power spectral density (PSD) of wall pressure probes are presented in Figs. 5 for the suction side. The plots display PSDs in terms of Strouhal number and airfoil chord, where the black vertical dashed lines indicate the mean separation and reattachment positions. For the higher Mach number flow, only the separation position is displayed, since there is no flow reattachment. Here, the Strouhal number St_c is based on the airfoil axial chord to compare the frequencies for all flows using the same length scales. For all cases, the PSD maps display regions with high spectral energy at low-frequencies. These regions are located upstream of the bubbles, near their leading edges, and when applicable, at the bubble trailing edges, near the reattachment locations. As previously discussed, increasing the inlet Mach number results in a downstream displacement

of the high-amplitude spectral content in the x-direction. For the cases with $M_\infty = 1.85$ and 2.00, one can observe an amplification of the spectral energy along the separation region, while for $M_\infty = 2.15$, at low-frequencies, similar levels of spectral energy are found between the bubble's leading and trailing edges.

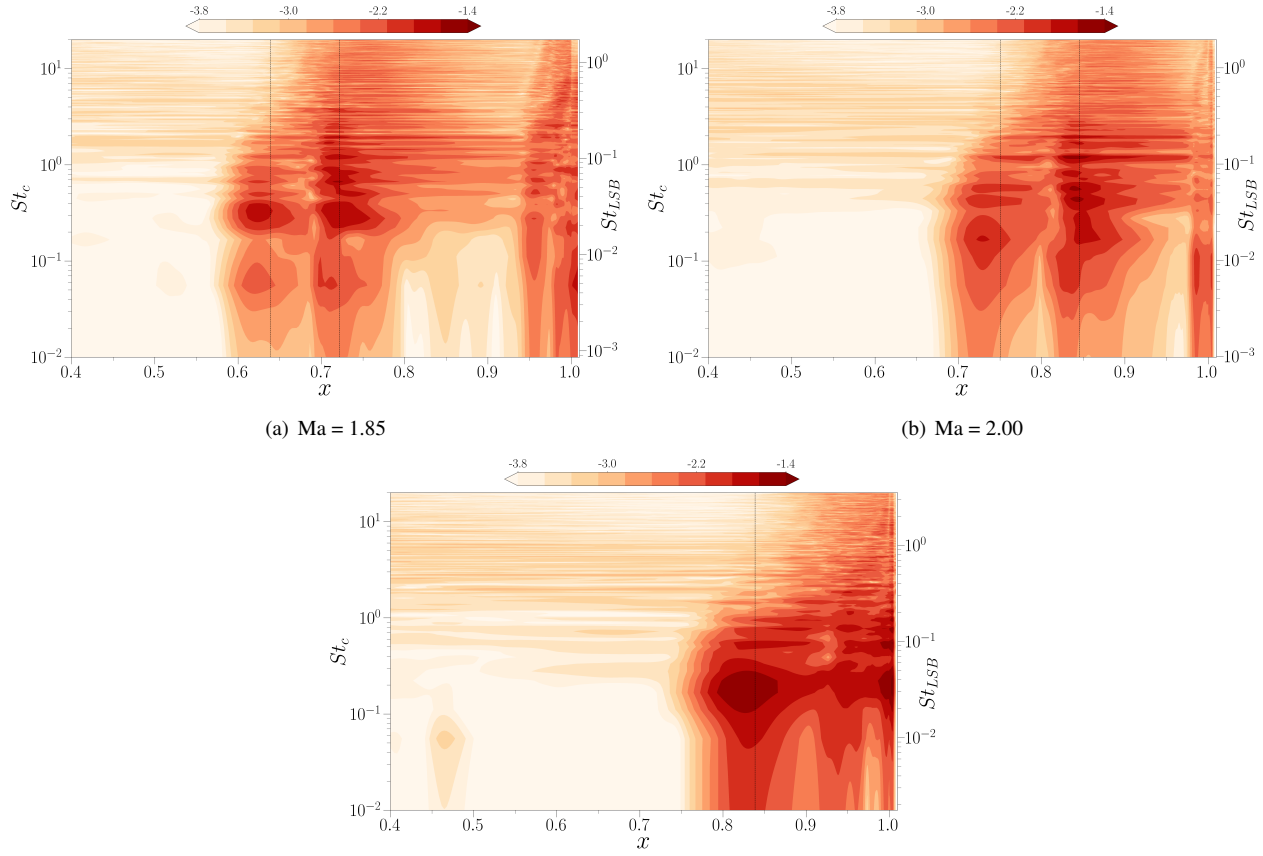

(a) Ma = 1.85

(b) Ma = 2.00

(c) Ma = 2.15

Figure 5. Power spectral density of wall pressure on the suction side for different inlet Mach numbers.

Regarding the characteristic frequencies excited by the SBLI system, for the case with $M_\infty = 1.85$, the peaks appear at $St_c \approx 0.27 - 0.38$, $St_c \approx 0.66$, and $St_c \approx 1.22$. As the Mach number is increased to 2.00, the dominant peaks are captured at $St_c \approx 0.16$, $St_c \approx 0.45 - 0.55$, and $St_c \approx 1.22$. Finally, for the $M_\infty = 2.15$ case, the most energetic peaks are observed at $St_c \approx 0.16 - 0.22$, $St_c \approx 0.55$, and $St_c \approx 0.75$. These results suggest that, in the present configuration, as the inlet Mach number increases, the SBLI system excites lower frequencies and this is most likely to be related to the larger separation bubbles. Despite these low-frequencies differences, they are associated to the same dynamics: the breathing of the separation bubble, oscillations of the compression waves and shocks, and flapping of the shear layer.

5. CONCLUSIONS

In this work, an assessment of shock-boundary layer interactions (SBLIs) is provided for a supersonic turbine cascade subjected to different inlet Mach numbers. Three Mach numbers are investigated being 1.85, 2.00 and 2.15. The effects of Mach number on the SBLIs are investigated using flow visualizations, mean flow quantities and spectral analysis. Each Mach number has different incidence of the oblique shock wave impinging at the surface, which, in turn, influences the SBLI region. For the M_∞ = 1.85 case, two SBLIs are present on the suction side, where the first is due to the incident shock, and the second occurs due to the reflected shock from the pressure side of the adjacent airfoil. This second shock also interacts with a separation bubble formed at the blunt trailing edge of the blade. For M_∞ = 2.00 and 2.15, a single SBLI occurs on the suction side. However, for the latter case, the SBLI occurs near the trailing edge and leads to a more complex interaction between the shock with the boundary layer, besides the trailing edge separation bubble.

The mean flow results indicate that the size of the separation bubble can be significantly affected by the variation in the Mach number. On the suction side, as the inlet Mach number is increased, the length of the separation bubble increases. In addition, by increasing the inlet Mach number, a smoother rise in pressure is observed, whereas a higher pressure jump is noticed for a lower inlet Mach number. On the other hand, on the pressure side, the separation bubbles have similar sizes and, as inlet Mach number is increased, the pressure jump across the shock also increases. It is important to note

that these effects can also have a spatial dependence due to the adverse/favorable pressure gradient, which will be a topic of future investigation.

The effects of the inlet Mach number on the low-frequency unsteadiness of the SBLI on the suction side is investigated by performing a spectral analysis of wall pressure probes. For all cases, the PSD maps show regions with high spectral energy at low-frequencies, where these regions are located upstream of the bubble, and near its leading and trailing edge. The results also indicate that, as the inlet Mach number increases, those regions with high-amplitude spectral content move downstream in the axial direction. For the case with $M_\infty = 1.85$, the peaks appear at $St_c \approx 0.27 - 0.38$, $St_c \approx 0.66$, and $St_c \approx 1.22$. As the Mach number is increased to 2.00, the dominant peaks are captured at $St_c \approx 0.16$, $St_c \approx 0.45 - 0.55$, and $St_c \approx 1.22$. Finally, for the $M_\infty = 2.15$ case, the most energetic peaks are observed at $St_c \approx 0.16 - 0.22$, $St_c \approx 0.55$, and $St_c \approx 0.75$. These results suggest that, in the present configuration, as the inlet Mach number increases, the SBLI system excites lower frequencies and this is most likely to be related to the larger separation bubbles.

6. ACKNOWLEDGEMENTS

The authors acknowledge the financial support received from Fundação de Amparo à Pesquisa do Estado de São Paulo, FAPESP, under Grants No. 2013/08293-7, No. 2019/26196-5, and No. 2021/06448-0. Numerical simulations were performed on the Stampede 2 machine at the Texas Advanced Computing Center, and on the Anvil machine at the Purdue Research Computing both via allocation MCH220001 from the Advanced Cyberinfrastructure Coordination Ecosystem: Services & Support (ACCESS) program, which is supported by National Science Foundation grants No. 2138259, No. 2138286, No. 2138307, No. 2137603, and No. 2138296.

7. REFERENCES

Adler, M.C. and Gaitonde, D.V., 2018. "Dynamic linear response of a shock/turbulent-boundary-layer interaction using constrained perturbations". *Journal of Fluid Mechanics*, Vol. 840, p. 291–341.

Baidya, R., Scharnowski, S., Bross, M. and Kähler, C.J., 2020. "Interactions between a shock and turbulent features in a Mach 2 compressible boundary layer". *Journal of Fluid Mechanics*, Vol. 893, p. A15.

Beam, R.M. and Warming, R.F., 1978. "An implicit factored scheme for the compressible Navier-Stokes equations". *AIAA Journal*, Vol. 16, No. 4, pp. 393–402. ISSN 0001-1452.

Beresh, S.J., Clemens, N.T. and Dolling, D.S., 2002. "Relationship between upstream turbulent boundary-layer velocity fluctuations and separation shock unsteadiness". *AIAA Journal*, Vol. 40, No. 12, pp. 2412–2422.

Bhaskaran, R. and Lele, S.K., 2010. "Large eddy simulation of free-stream turbulence effects on heat transfer to a high-pressure turbine cascade". *Journal of Turbulence*, Vol. 11, p. N6.

Clemens, N.T. and Narayanaswamy, V., 2014. "Low-frequency unsteadiness of shock wave/turbulent boundary layer interactions". *Annual Review of Fluid Mechanics*, Vol. 46, No. 1, pp. 469–492.

Cook, A.W., 2007. "Artificial fluid properties for large-eddy simulation of compressible turbulent mixing". *Physics of Fluids*, Vol. 19, No. 5, p. 055103.

Dupont, P., Haddad, C. and Debiève, J.F., 2006. "Space and time organization in a shock-induced separated boundary layer". *Journal of Fluid Mechanics*, Vol. 559, p. 255–277.

Dussauge, J.P., Dupont, P. and Debiève, J.F., 2006. "Unsteadiness in shock wave boundary layer interactions with separation". *Aerospace Science and Technology*, Vol. 10, No. 2, pp. 85–91. ISSN 1270-9638.

Gaitonde, D.V., 2015. "Progress in shock wave/boundary layer interactions". *Progress in Aerospace Sciences*, Vol. 72, pp. 80–99. ISSN 0376-0421.

Ganapathisubramani, B., Clemens, N.T. and Dolling, D.S., 2009. "Low-frequency dynamics of shock-induced separation in a compression ramp interaction". *Journal of Fluid Mechanics*, Vol. 636, p. 397–425.

Israeli, M. and Orszag, S.A., 1981. "Approximation of radiation boundary conditions". *Journal of Computational Physics*, Vol. 41, No. 1, pp. 115 – 135. ISSN 0021-9991.

Kawai, S., Shankar, S.K. and Lele, S.K., 2010. "Assessment of localized artificial diffusivity scheme for large-eddy simulation of compressible turbulent flows". *Journal of Computational Physics*, Vol. 229, No. 5, pp. 1739–1762. ISSN 0021-9991.

Klinner, J., Hergt, A., Grund, S. and Willert, C.E., 2019. "Experimental investigation of shock-induced separation and flow control in a transonic compressor cascade". *Experiments in Fluids*, Vol. 60, p. 96.

Lele, S.K., 1992. "Compact finite difference schemes with spectral-like resolution". *Journal of Computational Physics*, Vol. 103, No. 1, pp. 16–42. ISSN 0021-9991.

Liu, Z., Braun, J. and Paniagua, G., 2019. "Characterization of a supersonic turbine downstream of a rotating detonation combustor". *Journal of Engineering for Gas Turbines and Power*, Vol. 141, No. 3, p. 031501. ISSN 0742-4795.

Lui, H.F.S., Ricciardi, T.R., Wolf, W.R., Braun, J., Rahbari, I. and Paniagua, G., 2022. "Unsteadiness of shock-boundary layer interactions in a mach 2.0 supersonic turbine cascade". *Phys. Rev. Fluids*, Vol. 7, p. 094602.

Morgan, B., Duraisamy, K., Nguyen, N., Kawai, S. and Lele, S.K., 2013. "Flow physics and RANS modelling of oblique

shock/turbulent boundary layer interaction". *Journal of Fluid Mechanics*, Vol. 729, p. 231–284.

Nagarajan, S., Lele, S.K. and Ferziger, J.H., 2003. "A robust high-order compact method for large eddy simulation". *Journal of Computational Physics*, Vol. 191, No. 2, pp. 392–419. ISSN 0021-9991.

Nichols, J.W., Larsson, J., Bernardini, M. and Pirozzoli, S., 2017. "Stability and modal analysis of shock/boundary layer interactions". *Theoretical and Computational Fluid Dynamics*, Vol. 31, No. 1, pp. 33–50.

Paniagua, G., Iorio, M., Vinha, N. and Sousa, J., 2014. "Design and analysis of pioneering high supersonic axial turbines". *International Journal of Mechanical Sciences*, Vol. 89, pp. 65 – 77. ISSN 0020-7403.

Pirozzoli, S. and Grasso, F., 2006. "Direct numerical simulation of impinging shock wave/turbulent boundary layer interaction at M=2.25". *Physics of Fluids*, Vol. 18, No. 6, p. 065113.

Poinsot, T. and Lele, S., 1992. "Boundary conditions for direct simulations of compressible viscous flows". *Journal of Computational Physics*, Vol. 101, No. 1, pp. 104 – 129. ISSN 0021-9991.

Porter, K.M. and Poggie, J., 2019. "Selective upstream influence on the unsteadiness of a separated turbulent compression ramp flow". *Physics of Fluids*, Vol. 31, No. 1, p. 016104.

Priebe, S. and Martín, M.P., 2012. "Low-frequency unsteadiness in shock wave–turbulent boundary layer interaction". *Journal of Fluid Mechanics*, Vol. 699, p. 1–49.

Rubini, D., Xu, L., Rosic, B. and Johannesdahl, H., 2021. "A new turbomachine for clean and sustainable hydrocarbon cracking". *Journal of Engineering for Gas Turbines and Power*, Vol. 144, No. 2. ISSN 0742-4795.

Sandberg, R.D. and Michelassi, V., 2022. "Fluid dynamics of axial turbomachinery: Blade- and stage-level simulations and models". *Annual Review of Fluid Mechanics*, Vol. 54, No. 1, pp. 255–285.

Sansica, A., 2015. *Stability and unsteadiness of transitional shock-wave/boundary-layer interactions in supersonic flows*. Ph.D. thesis, University of Southampton.

Sousa, J., Paniagua, G. and Morata, E.C., 2017. "Thermodynamic analysis of a gas turbine engine with a rotating detonation combustor". *Applied Energy*, Vol. 195, pp. 247 – 256. ISSN 0306-2619.

Touber, E. and Sandham, N.D., 2009. "Large-eddy simulation of low-frequency unsteadiness in a turbulent shock-induced separation bubble". *Theoretical and Computational Fluid Dynamics*, Vol. 23, pp. 79–107.

Waindim, M. and Gaitonde, D., 2016. "A body-force based method to generate supersonic equilibrium turbulent boundary layer profiles". *Journal of Computational Physics*, Vol. 304, pp. 1–26. ISSN 0021-9991.

8. RESPONSIBILITY NOTICE

The authors are solely responsible for the printed material included in this paper.